COARSENING IN TWO-DIMENSIONAL SOAP FROTHS AND THE LARGE-Q POTTS MODEL

GARY S. GREST*, JAMES A. GLAZIER#†, MICHAEL P. ANDERSON*, ELIZABETH A. HOLM+ AND DAVID J. SROLOVITZ+
*Corporate Research Science Laboratory, Exxon Research and Engineering Company, Annandale, NJ 08801
#Research Institute of Electrical Communications, Tohoku University, Sendai 980, Japan
+Department of Material Science and Engineering, The University of Michigan, Ann Arbor, Michigan 48109

ABSTRACT

A detailed comparison between the experimental evolution of a two-dimensional soap froth and the large Q state Potts model is presented. The pattern evolution starting from identical initial conditions will be compared as well as a variety of distribution functions and correlations of the two systems. Simulations on different lattices show that the discrete lattice of the Potts model causes deviations from universal domain growth by weakening the vertex angle boundary conditions that form the basis of von Neumann's law. We show that the anisotropy inherent in a discrete lattice simulation, which masks the underlying 'universal' grain growth, can be overcome by increasing the range of the interaction between spins or increasing the temperature. Excellent overall agreement between the kinetics, topological distributions and domain size distributions between the low lattice anisotropy Potts-model simulations and the soap froth suggests that the Potts model is useful for studying domain growth in a wide variety of physical systems.

Introduction

There are many experimental systems which exhibit grain growth or coarsening in time, including metallic and ceramic recrystallization, magnetic materials, lipid monolayers, biological aggregates and soap froths [1-3]. There are a similar variety of models for coarsening including simple mean field theories which look only at distributions [4,5], mean field theories which include topology [6-8], "exact" models which calculate the motions of boundaries or vertices [9-12], and the Potts model which takes a microscopic approach to modeling [13-17]. In all such systems surface energy driven diffusion leads to the motion of curved boundary walls causing certain grains to grow while others shrink and disappear. The result is a gradual increase in the overall length scale of the grains. This basic dynamics is influenced by the geometrical constraint that vertices are three-fold connected to produce a family of typical patterns of coordination number three. Independent of the initial configuration of domains or bubbles, these systems gradually become disordered with time-invariant distributions of the number of sides per bubble and bubble areas (a scaling state). Besides the intrinsic interest of the transition from order to disorder, coarsening has many technological applications in metallurgy, for example in the design of materials with particular mechanical properties. The coarsening properties of metals have therefore been widely studied [2]. Unfortunately, in many cases, secondary effects such as impurity segregation and crystalline anisotropy mask the underlying universal features of two-dimensional coarsening.

†Permanent Address: Department of Physics, The University of Notre Dame, Notre Dame, IN 46556

Mat. Res. Soc. Symp. Proc. Vol. 237. ©1992 Materials Research Society

To try to sort out the underlying ideal coarsening behavior, we turn to the two-dimensional soap froth which was first proposed by Smith [8] as a particularly simple example of a cellular system which coarsens in time [19-24]. It appears that soap froths obey a simple dynamical law known as von Neumann's law [25],

$$\frac{da_n}{dt} = \kappa(n-6)$$

where a_n is the area of an n-sided bubble and κ is a diffusion constant. If von Neumann's law were all there were to froth evolution, the problem would be trivial; however, when bubbles disappear, their neighbors gain or lose sides, resulting in continual changes in each bubble's rate of growth or shrinkage. The difficulty in most models is to treat the redistribution of sides correctly.

There have been a number of vertex and boundary dynamics models [9-12] which have been developed to describe the basic physics of a soap froth, in which gas diffuses across well defined soap films. Potts model simulations, on the other hand, take a quasi-microscopic metallurgical view of coarsening in which a lattice is used to discretize the continuum microstructure. As in real coarsening, curvature of domain boundaries leads to increased wall energy on the convex side and hence to wall migration. Coarsening results because few-sided grains have larger total curvatures than many-sided grains and hence shrink.

The Potts model is space filling, unlike some vertex models and trades the deterministic diffusion of gas across a soap film for the probabilistic motion of an interface between domains of different spin types. However, Grest et al. [15] have shown numerically that the $Q = \infty$ state Potts model obeys von Neumann's law on average. If the redistribution of sides in the model is similar to that in an actual froth, we expect good agreement between the temporal evolution of the two systems.

One difference between the Potts model and a real soap froth is the Potts model's orientationally anisotropic boundary energy. We show the anisotropy in a Wulff plot (Fig. 1) at T = 0 for three different ranges of interaction. The effect of the anisotrophy is to absorb wall curvature at vertices and hence to reduce the effective force driving boundary motion. In the case of the nearest-neighbor square lattice (Fig. 1(b)), the anisotropy is so strong that the boundary walls flatten, and coarsening rapidly slows and stops [13]. We therefore work with nearest and next-nearest-neighbor triangular and next-nearest-neighbor square lattices which have lower anisotropy. Another difference between the froth and the Potts

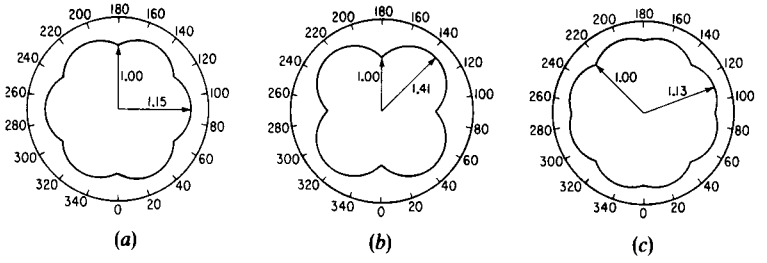

Figure 1 Potts model anisotropies. Energy per unit surface length as a function of surface angle (a) for a nearest-neighbor hexagonal lattice (b) for a nearest-neighbor square lattice and (c) for a next-nearest neighbor square lattice. The labelled arrows show energy extrema and values.

model is that the diffusion time of gas across a soap film is much slower than the equilibration time of the film along its length, while in the Potts model and most metals the two times are the same. Thus, soap films are closer in shape to true equilibrium surfaces than are grain boundaries in the Potts model and metals. In this respect our model differs significantly from that of Wejchert et al. [16], who used a double time step, first applying von Neuman's law to fix target areas for each grain and then using Potts model evolution to relax the grain boundaries to an equilibrium configuration.

In this paper, we show that while lattice anisotropy is unquestionably present in the Potts model, the main features of domain growth (e.g., the temporal scaling of domain size) are unaffected by small changes in anisotropy. In fact, the overall agreement between the evolution of a soap froth and a Potts model starting from similar conditions is very good. Lattice anisotropy does have an important effect on the scaling state topological and area distribution functions. We [17] find that all moments of these distributions decrease with decreasing anisotropy and approach the results for soap froth in the limit of zero anisotropy, suggesting that there is an underlying 'universal' grain growth which is often masked by anisotropy effects.

Experimental Procedure and Model

In the soap froth experiments, a cell (typically 8.5 x 11.5 x 1/8 inches) is filled with a well ordered array of small bubbles (typically 10,000 bubbles) [20]. The excess fluid in the films accumulates on the top and bottom plates of the cell in Plateau borders, which are much broader than the films themselves. These borders may change the evolution of the froth (there is no reason to suppose that they have a linear bending energy for example) but they do allow one to easily record the pattern by placing it level on a photocopier, and photocopying periodically. Photocopying heats the froth and can occasionally cause walls to break. The total number of walls broken during a run is less than 0.1% of the total side redistribution, but nevertheless results in a slightly greater number of very many-sided bubbles. The only real control parameters are the temperature, type and pressure of the gas and the total volume of fluid in the Plateau borders. The detailed properties of the fluid are not important as long as its viscosity is small.

In the Potts model, a spin $\sigma(i,j)$ is defined for each lattice site. All lattice points lying with a given grain are assigned the same value of spin, with a different spin for each grain. Since we denote the number of different degenerate spins in the model by Q, we have Q = number of grains Potts model. However, since each grain is separately labelled, we generally refer to it as the Q = ∞ model. The Potts Hamiltonian is

$$H = J \sum_{(i,j)(i',j')} 1-\delta_{\sigma(i,j)\sigma(i',j')} \qquad (1)$$

where J is a positive constant, δ is the Kronecker delta function, $1 \leq \sigma(i,j) \leq N_d$ denotes the orientation of the spin at site (i,j), N_d is the number of domains in the system at the beginning of the simulation, and (i,j), (i',j') represents (i,j),(i',j') neighbors. Evolution proceeds by a Monte Carlo procedure in which a spin is selected at random and converted to a new random orientation with probability $p=\exp(-\Delta E/kT)$ where ΔE is the change in system energy produced by the reorientation. After each reorientation attempt, time is incremented by $1/N_\sigma$ Monte Carlo steps (MCS), where N_σ is the number of lattice spin sites in the system. At $T > T_c$ the system is disordered, while at $T < T_c$ a well-defined domain structure evolves. At T = 0, these domains are simply connected; however, at finite temperatures small domains may nucleate within a larger domain. In order

to alleviate the effects of these fluctuations, we quench each finite temperature simulation to T = 0 for a short time prior to enumerating the domain size and side distributions. Since the average number of sides per domain $\langle n \rangle = 6$ for simply connected domains, the duration of the quench is adjusted such that $5.98 < \langle n \rangle < 6.02$.

We study the anisotropy of the Potts model by performing identical simulations on a variety of lattices with different anisotropies and at a variety of temperatures. We characterize the anisotropy by the ratio of the highest-to the lowest-energy domain boundary orientations. The highest possible anisotropy occurs for the nearest-neighbor honeycomb lattice. However, steady state domain growth does not occur on this lattice at any temperature. We therefore confine our study to the nearest- and next-nearest-neighbor square lattices [s(1) and s(1,2), respectively] and the nearest-and next-nearest-neighbor triangular lattices [t(1) and t(1,2), respectively]. The lattice anisotropies η for these lattices are $\eta_s(1)=1.414$, $\eta_s(1,2)=1.116$, $\eta_t(1)=1.154$, and $\eta_t(1,2)=1.057$. We used two different types of Potts models in our simulations. For direct comparison to experiments on soap froths, we used a second nearest neighbor interaction on a 600x500 square lattice with open boundary conditions. To check the effect of anisotropy, we used a 200x200 lattice with periodic boundary conditions. Results for the nearest neighbor triangular lattice on a 200x200 lattice agreed very well with earlier work on a 1000x1000 lattice with Q=48 [15]. These latter simulations were performed by quenching from $T \gg T_c$ to $T < T_c$. The results presented are averaged over ten independent simulations.

Kinetics

The basic measure of the evolution of domain structure is the average domain size as a function of time. Any system obeying von Neumann's law reaches a scaling state in which

$$\langle a(t) \rangle^{1/\alpha} - \langle a(0) \rangle^{1/\alpha} = \gamma t, \tag{2a}$$

$$\langle a(t) \rangle \sim t^{\alpha} \tag{2b}$$

where Eq. (2b) is valid for $\langle a(t) \rangle \gg \langle a(0) \rangle$, γ is a positive constant, and $\alpha=1$. Deviations from $\alpha=1$ are common experimentally and indicate the presence of additional effects: for example, finite fluid fraction in soap froths [21] and impurities in metals [2] result in lower growth rates at long times and hence lower exponents. Generally, the domain growth exponent α gradually increases as the system approaches steady state [20].

Figure 2 shows the temporal evolution of the mean domain area (a). In the t(1,2), s(1,2), and t(1) lattices at all temperatures, the rate of growth of a increases monotonically in time to a value consistent with the large-system asymptotic exponent $\alpha=1$ [15]. For the s(1) lattice, zero temperature domain growth halts when the domain vertices absorb all initial wall curvature; however, domain wall fluctuations which occur at any finite temperature enable domain growth to proceed to completion [13,26]. The effect of lattice anisotropy on domain growth is shown in Fig. 2a. Assuming that the anisotropy is not too large for domain growth to occur [as in s(1) at T=0], increases in lattice anisotropy decrease the growth rate at early time ($t < 10^2$ MCS). Following this very early growth rate dependence on lattice anisotropy, the domain coarsening rate becomes independent of anisotropy; hence, all of the curves in Fig. 2a are parallel at later times ($t > 10^2$ MCS). Results for $T \neq 0$ are shown in Fig. 2b for the nearest neighbor triangular lattice. In this case, finite T has little effect on the kinetics.

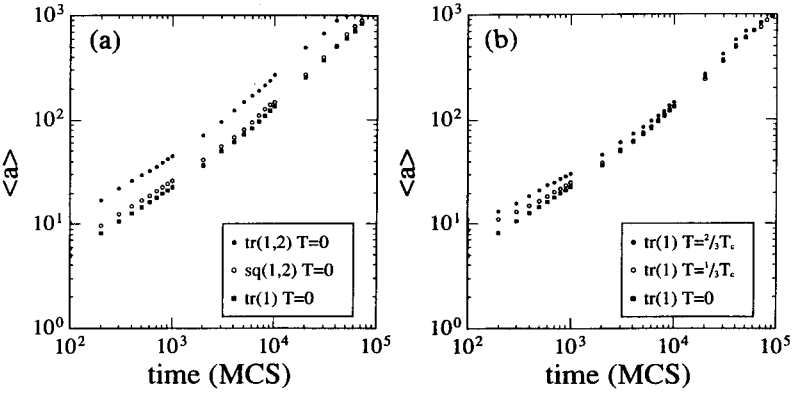

Figure 2 Mean domain area versus time for the Potts model (a) t(1), t(1,2) and s(1,2) at T=0 and (b) t(1) for three temperatures.

These results clearly show that the discreteness of the lattice is unimportant to domain growth kinetics in the long-time regime, since all of the simulations tend to the same scaling behavior at long times or large domain size. In contrast, at early times, decreasing lattice anisotropy or increasing temperature tend to reduce the kinetic effects of lattice discreteness and increase growth rates. Likewise, the discreteness of the atomic lattice in grain growth, in effect, decreases with increasing temperature, as evinced in the experimentally observed increase in grain growth exponents with increasing temperature [27]. However, we also find that temperature and lattice anisotropy are not equivalent variables.

To compare more directly the temporal evolution of the soap froth and the Potts model, we [1] carried our two runs using digitized soap froth images at t=0 minutes (2490 grains) and t=2044 minutes (1175 grains) as the starting patterns. The t=0 minutes initial pattern was composed almost entirely of hexagonal bubbles of nearly equal area while the t=2044 minute pattern had evolved sufficiently that there were few islands of six-sided bubble remaining from the initial fill. The qualitative features of the disordering were similar for the two simulations and the experiment. We compare the experiment and the t=2044 minutes simulation in Fig. 3, though the differing boundary conditions (the sample of the froth was taken from the bulk whereas the simulation had open boundary conditions) resulted in a rapid divergence between the actual patterns. In the simulation starting from the t=2044 minutes soap froth image the disappearance of residual order occurred in both systems at comparable length scales (after an increase of approximately one order of magnitude), and the qualitative patterns remained comparable (We use the conversion that time is the number of MC steps times 0.32, $t=t_{MC}*0.32$). Regardless of the initial random seed, the simulation starting from the t=0 minutes soap froth image retained its hexagonal pattern for much longer than the froth. This difference in side redistribution comes about because of angle effects due to lattice anisotropy in the Potts model. These simulations were run on the square lattice with nearest- and next-nearest neighbor interactions. Due to the lattice anisotropy ($\eta_S(1,2)=1.116$) for this case, six-sided bubbles are less likely to change their number of sides in the model than in the experimental soap froth. Once the blocks of hexagons disappeared however, the rate of evolution caught up and the long term states of the t=0 and t=2044 minutes square lattice Potts model simulations are indistinguishable. In Fig. 4 we compare the average bubble size versus

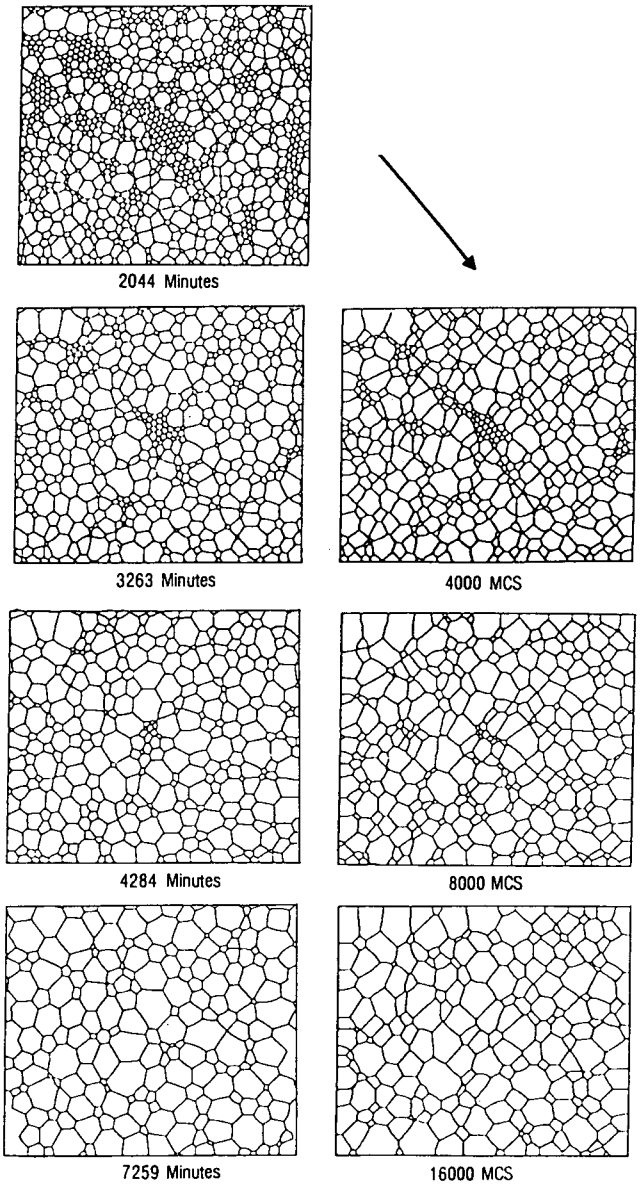

Figure 3 Evolution of soap froth (left) and the square lattice Potts model (right) using the state of the soap froth at t = 2044 minutes as the initial condition.

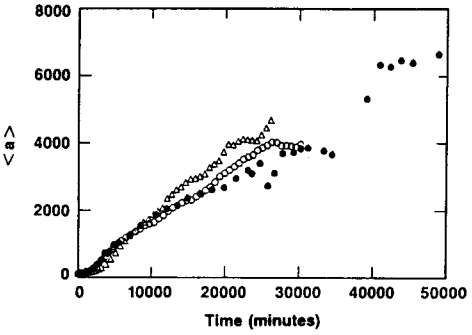

Figure 4 Average bubble area versus time for soap froth (bullets), square lattice Potts model simulation starting from the digitized soap froth image at t = 2044 minutes (open circles) and square lattice Potts model simulation starting from the digitized soap froth image at t=0 minutes (triangles).

time for the froth and Potts model simulations on a square lattice s(1,2). We found essentially exact agreement between the froth and the t=2044 minutes simulation up to 20,000 minutes where the statistics are best, after which both showed fluctuations. The initial rate of area growth of the t=0 minutes simulation was significantly slower than the froth, due to the lattice anisotropy. In both cases the typical qualitative dynamics for coarsening of an initially ordered froth appeared: slow initial evolution, followed by rapid growth during which any residual order disappeared, and a long term tail with slower power law growth [20]. The growth exponent of both simulations was slightly higher than in the froth, but all were consistent with linear growth in time, i.e. α=1. Bolton and Weaire [12] have shown from their simulations for a soap froth with Plateau borders that the experimentally measured lower growth exponent is due to an increase of Plateau border width during experiments in sealed cells. Earlier experiments [21] in small sealed cells gave exponents α<1. However, our experiments [1] on larger cells and those of Stavans [24] on a drained cell, give α=1 consistent with the Potts model.

Distribution Functions

Besides the mean bubble area, the two basic measures of the state of a froth are the distribution of the number of sides (ρ(n), the probability of a randomly selected bubble has n sides) and the normalized area distribution (ρ(a/<a>), the probability that a bubble has an area which is a given fraction of the mean bubble area). We define the mth moment of the side distribution as:

$$\mu_m(T) = \sum_{n=2,\infty} \rho(n)(n-\langle n\rangle)^m , \qquad (3)$$

where <n> is the average number of sides of a bubble in the pattern (for infinite patterns <n>=6). We sum from n=2 because two-sided grains can occur in metallic and other materials. Moments higher than μ_2 are sensitive to the large n tail of the distribution, which is subject to counting error. A similar integral expression can be used to determine μ_m(A), the mth moment of the area distribution.

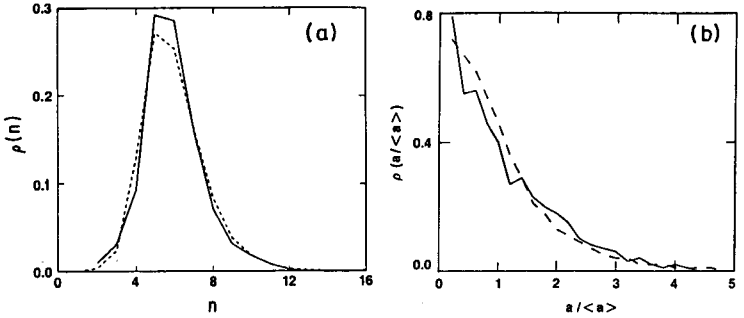

Figure 5(a) Side distribution in the scaling state for soap froth (solid) and triangular lattice Potts model (dashed). (b) Fractional area distribution in the scaling state for soap froth (solid) and triangular lattice Potts model (dashed).

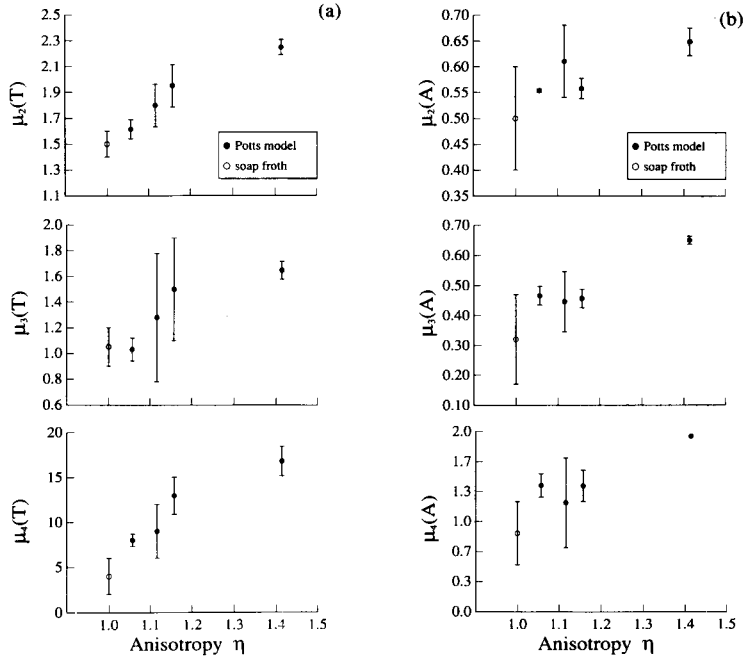

Figure 6 Effect of lattice anisotropy on the moments of scaling state domain topology (a) and domain area distributions (b). All moments decrease with decreasing anisotropy. Error bars indicate approximate range of fluctuations during the scaling state. Open circles denote the best experimental values for the two-dimensional soap froth.

At approximately 10,000 minutes (see Fig. 4), just after the rate of evolution rolls over to a power law, the experimental distribution becomes essentially time independent, confirming the existence of the scaling state noted by Stavans and Glazier (Q=48) [21]. We plot the scaling distribution for the nearest neighbor triangular lattice Potts model simulation (Q=48) and for the froth in Fig. 5a. While $\rho(n)$ for the simulation lies within the range of experimentally measured values for each n, the froth has fewer four-and many-sided bubbles. Interestingly, the Q=48 triangular lattice Potts model with wall breakage gives nearly identical distributions to the Q=∞ square lattice Potts model without. Results for the fractional area distribution are shown in Fig. 5b.

We find that the moments μ_m are sensitive to the anisotropy and approach the results for the soap froth only in the limit $\eta \to 1$. Results for the first three moments increase monotonically with increasing anisotropy. In Fig. 6a, we show the results from simulations on four lattices as well as experimental data obtained from the soap froth experiments. The soap froth results are in good overall agreement with the simulation data on the t(1,2) lattice. This is not surprising since the anisotropy for soap froth should be identically unity (i.e., isotropic) and the t(1,2) has the smallest anisotropy of any of the lattices investigated (i.e., about 1.06). The experimental topological moments obtained by Fradkov et al. [28] for two-dimensional grain growth in Al + 10^{-4} Mg foil at 460°C are substantially larger than all corresponding scaling state Potts-model values. The large values of the moments may reflect an equilibration transient, growth retardation due to the interaction of the grain boundaries with the surface, retardation due to impurity drag, or inherent anisotropy associated with the atomic lattice.

In Fig. 6b we also plot the moments of the domain area distributions $\mu_m(A)$ as a function of lattice anisotropy. The moments tend to increase monotonically with the lattice anisotropy, although the scatter in the data is much more pronounced than for the topological moments. Comparison with the soap froth data again shows that best agreement is obtained in the limit that the lattice anisotropy tends to one. Unfortunately, the moments of the Al thin film area distributions are not available.

Correlations

Of the aggregate quantities derivable from the area distribution functions, the average radius of an n-sided bubble as a function of n is the most useful. If we plot $r_n = \langle a_n^{1/2} \rangle / \langle a^{1/2} \rangle$ (Fig. 7) the graph is

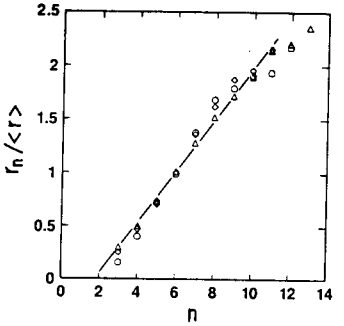

Figure 7 Fractional radius in the scaling state of an n-sided grain versus n for the soap froth (circles) and the square lattice s(1,2) with nearest and next nearest neighbor interactions (diamonds) and triangular lattice t(1) with nearest neighbor interaction (triangles) Potts models.

essentially linear, with just a hint of S-curve rollover for large n [29,30]. In this case, because of the scarcity of many-sided bubbles, we may well be observing a selection effect: large many-sided bubbles are more likely to intersect the frame boundary than small bubbles and are hence more likely to be excluded from consideration, resulting in a low apparent size for large n. The soap froth and s(1,2) and t(1) Potts model simulations give essentially identical results in the scaling regime. The metal foil of Fradkov et al. has slightly larger many-sided grains [28].

The simplest side correlation function to measure is the average number of sides of the neighbors of an n-sided bubble, m(n). Weaire has argued on physical grounds that:

$$m(n)=6-a+(6a+\mu_2)/n, \qquad (4)$$

where μ_2 is the second moment of the side distribution and a is a constant of order one [31]. Peshkin, Strandburg and Rivier [8] have recently shown that this result follows directly from a maximum-entropy approach. It is observed to hold both in the froth and the Potts model [1,22]. Other distributions, including $\rho_m(n)$, the probability that a bubble next to an m-sided bubble has n sides, have also been determined for both the soap froth and Potts models. The results are presented in Ref. [1]. As expected we find that few-sided bubbles tend to be near many-sided bubbles. The converse is not true, however. Six-sided bubbles cluster together and seven-sided bubbles attract six-sided bubbles. Even more surprising, the distribution of neighbors of eight-sided bubbles is essentially the same as the total distribution. Discounting the bias towards many-and few-sided bubbles that we have noted in the simulation, the behavior of the distributions as a function of m is identical for the Potts model and the froth.

Conclusions

The excellent overall agreement (kinetics, topological distribution, domain size distributions) between the low lattice anisotropy Potts-model simulations and the soap froth show that the Potts model is a useful analog system for studying domain growth in a wide variety of physical systems. Additionally, the similarity between soap froth evolution, grain growth, and Potts-model domain growth demonstrate the universality of domain growth in highly degenerate systems and the general applicability of the von Neumann construction. A discrete lattice causes deviations from universal domain growth behavior by weakening the vertex angle boundary conditions which form the basis of von Neumann's law. The anisotropy inherent in discrete lattice simulations can be overcome by smoothing the Wulff plot of the lattice (e.g., by extending spin interactions to longer range) or by elevating the temperature at which the simulation is performed.

References

1. J. A. Glazier, M. P. Anderson, and G. S. Grest, Phil. Mag. B 62, 615 (1990); J. A. Glazier, G. S. Grest and M. P. Anderson, in Simulation and Theory of Evolving Microstructures, edited by M. P. Anderson and A. D. Rollett (The Minerals, Metals and Materials Society) Warrendale, PA., (1990) p. 41.
2. P. A. Beck, Adv. Phys. 3, 245 (1954); H. V. Atkinson, Acta Met. 36, 469 (1988).
3. D. Weaire and N. Rivier, Contemp. Phys. 25, 59 (1984).
4. M. Marder, Phys. Rev. A 36, 438 (1987).
5. V. E. Fradkov, D. G. Udler, and R. E. Kris, Philos. Mag. Letters 58, 670 (1988).
6. V. E. Fradkov, L. S. Shvindlerman, and D. G. Udler, Scripta Met. 19, 1285 (1985).

7. C. W. J. Beenakker, Phys. Rev. Lett. 57, 2454 (1986); Phys. Rev. A 37, 1697 (1988).
8. M. A. Peshkin, K. J. Strandburg and N. Rivier, Phys. Rev. Lett. 67, 1803 (1991).
9. H. J. Frost and C. V. Thompson, in Computer Simulation of Microstructural Evolution, edited by D. J. Srolovitz (The Metallurgical Society, Warrendale, PA, 1986), p. 33; H. J. Frost, C. V. Thompson, C. L. Howe and J. Whang, Scripta. Metal. 22 65 (1988).
10. D. Weaire and J. P. Kermode, Philos. Mag. B 47, L29 (1983); Phil. Mag. B 48, 245 (1983); ibid. 50, 379 (1984);D. Weaire and H. Lei, Phil. Mag. Lett. 62, 427 (1990).
11. K. Kawasaki, T. Nagai, and K. Nakashima, Phil. Mag. B 60, 1399 (1989).
12. F. Bolton and D. Weaire, Phys. Rev. Lett. 65, 3449 (1990); Phil. Mag B 63, 795 (1991).
13. M. P. Anderson, D. J. Srolovitz, G. S. Grest, and P. S. Sahni, Acta Met. 32, 783 (1984).
14. D. J. Srolovitz, M. P. Anderson, P. S. Sahni, and G. S. Grest, Acta Met. 32, 793 (1984).
15. G. S. Grest, D. J. Srolovitz, and M. P. Anderson, Phys. Rev. B 38, 4752 (1988).
16. J. Wejchert, D. Weaire, and J. P. Kermode, Philos. Mag. B 53, 15 (1986).
17. E. A. Holm, J. A. Glazier, D. J. Srolovitz, and G. S. Grest, Phys. Rev. A 43, 2662 (1991).
18. C. S. Smith, in Metal Interfaces, (American Society for Metals, Cleveland, 1952), p.65.
19. Tingliang Fu, "A Study of Two-Dimensional Soap Froths" (M.S. thesis, Trinity College, Dublin, 1986).
20. J. A. Glazier, S. P. Gross, and J. Stavans, Phys. Rev. A 36, 306 (1987).
21. J. A. Glazier and J. Stavans, Phys. Rev. A 40, 7398 (1989).
22. J. Stavans and J. A. Glazier, Phys. Rev. Lett. 62, 1318 (1989).
23. J. A. Glazier, Ph.D. thesis, University of Chicago, 1989.
24. J. Stavans, Phys. Rev. A 42, 5049 (1990).
25. J. von Neumann, in Metal Interfaces (American Society for Metals, Cleveland, 1952), p. 108.
26. Z. W. Lai, G. F. Mazenko and O. T. Valls, Phys. Rev. B 37, 9481 (1988).
27. F. Haessner and S. Hofmann, in Recrystallization of Metallic Materials, edited by F. Haessner (Riederu Verlag, Stuttgart, 1978), p. 76.
28. V. E. Fradkov, A. S. Kravchenko, and L. S. Shvindlerman, Scipta Met. 19, 1291 (1985).
29. F. T. Lewis, Anatomical Record 38, 341 (1928).
30. F. Feltham, Acta Met. 5, 97 (1957).
31. C. J. Lambert and D. Weaire, Metallography 14, 307 (1981).